


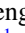

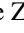
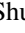
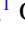



Spin dynamics in the axion insulator candidate EuIn_2As_2 Qiong Wu ^{1,*}, Tianchen Hu ¹, Dong Wu ², Rongsheng Li ¹, Li Yue ¹, Sijie Zhang ¹, Shuxiang Xu ¹, Qiaomei Liu ¹,
Tao Dong¹ and Nanlin Wang ^{1,2,†}¹International Center for Quantum Materials, School of Physics, Peking University, Beijing 100871, China²Beijing Academy of Quantum Information Sciences, Beijing 100193, China

(Received 26 September 2022; revised 4 January 2023; accepted 12 April 2023; published 10 May 2023)

We report the investigation of spin dynamics in the antiferromagnetic metal EuIn_2As_2 with the Zintl phase by using time-resolved magneto-optical Kerr effect (TR-MOKE) and transient reflectivity spectroscopy. In TR-MOKE measurement, we observe a spin precession mode with a frequency of about 18 GHz below 1.4 T and a new emerging coherent acoustic phonon mode near 35 GHz at a higher field where the latter shows a field-independent behavior. With temperature increasing, the spin precession disappears above Néel temperature T_N , whereas the acoustic phonon persists up to 25 K due to existence of magnetic-field-induced polarized paramagnetism. In contrast, the quasiparticle dynamics of EuIn_2As_2 does not show dramatic change in the vicinity of T_N . By comparing the spin and quasiparticle dynamics, we attribute the appearance of an acoustic phonon in TR-MOKE to photoinduced transient perturbation of magneto-optical coefficient. Our paper provides an in-depth investigation on the dynamical magnetic properties and broadens the understanding of the EuIn_2As_2 system.

DOI: [10.1103/PhysRevB.107.174411](https://doi.org/10.1103/PhysRevB.107.174411)

I. INTRODUCTION

Zintl phases represent the intermetallic compounds composed of metals with very different electronegativities. Theoretically, there is a complete transfer of valence electrons among the alkali or alkaline atoms to make all components satisfy the eight-electron closed-shell configuration [1,2]. However, because the valence electron transfer cannot be formed completely, Zintl phase materials are generally in the region between metal and semiconductor [3,4]. Therefore, Zintl phases often have very fertile physical properties, such as superconductivity [5], magnetoresistance [6], and mixed valency [7]. Moreover, coexistence of high electrical conductivity and low thermal conductivity [8] makes Zintl phases good thermoelectric materials. Abundant physical properties and superior thermoelectric effect, therefore, greatly increase the application value of Zintl phases.

EuIn_2As_2 is a three-dimensional antiferromagnetic (AFM) metal with the Zintl phase, which crystalizes in the hexagonal $P6_3/mmc$ space group [6] and contains the staggerly stacked Eu and In_2As_2 layers along the c axis. Below its Néel temperature $T_N \approx 16$ K, EuIn_2As_2 turns into the AFM state and shows giant magnetic resistance [6,9] where the spins of Eu^{2+} in one layer are ferromagnetically arranged within the ab plane, whereas the interlayer coupling is AFM. Photoemission investigation reveals the signature of band inversion in the AFM phase [10,11]. With applying the magnetic field above 0.9 T on the ab plane or about 2 T along the c axis, the spins in EuIn_2As_2 can be fully polarized [12]. A very recent investigation argues that the spin in EuIn_2As_2 should be in the helical arrangement [13]. With applying pressure on

EuIn_2As_2 , there is a significant increase in T_N from 16 to 65 K [14].

Significantly, EuIn_2As_2 is predicted to be an intrinsic axion insulator candidate, whose topological surface state can be tuned by changing the direction of staggered magnetic moments [15,16]. Since the discovery of a topological insulator [17,18], topological properties in condensed-matter physics have attracted great attention. Topological nontrivial states, such as the Dirac fermion [19,20], the Weyl fermion [21–23], and the Majorana fermion [24,25], etc, are protected by structure symmetry and cannot be destroyed by perturbation. These topological electronic states have a very important application prospect in the future low-dissipation electronic transport and new memory devices. Moreover, appearance of magnetism in topological materials can break the time-reversal symmetry, cause large Berry curvature, and finally lead to more interesting quantum states and novel physical phenomena, such as the anomalous Hall effect [26,27], topological Hall effect, magnetic Weyl semimetals [28–30], and axion insulator states [31–33]. Different from materials of particular thickness or stacking configuration [33], EuIn_2As_2 is an ideal platform to investigate the axion electrodynamics.

Magnetism plays an crucial role in determining the topological properties of EuIn_2As_2 . Kerr rotation spectroscopy is a well-known optical method to investigate the magnetic properties on condensed matters. The linearly polarized incident light can be regarded as sum of left- and right-circularly polarized light beams. In a magnetic-ordered sample, the local effective magnetic field makes the electrons respond differently to two types of circularly polarized light beams (i.e., the optical conductivity is different for two circular polarized beams). Thus, the polarization angle or ellipticity of reflected summed light beam yields slight variation [34]. Comparing with the traditional transport or susceptibility measurements,

*qwu20@pku.edu.cn

†nlwang@pku.edu.cn

Kerr rotation measurement possesses high spatial [35], layer number [36,37], and rotation angle resolution [38], and even owns energy resolution [39]. Furthermore, ultrafast lasers can interact with magnetic order and lead to several fascinating transient states [40], including ultrafast demagnetization [41,42], coherent magnetic precession [43], and even laser-induced phase transitions between two magnetic states [44]. The three-temperature model was widely used to phenomenologically elucidate the laser-induced magnetization dynamics: femtosecond pulse warms electron to hundreds of Kelvin, subsequently, the energy is transmitted to spin and lattice degree. The spin temperature increases and equilibrium orientation accordingly changes, leading to the spin rotation around the new equilibrium position and formation of spin wave. Although the static magnetical characteristic of EuIn_2As_2 has been thoroughly studied, its nonequilibrium dynamics behavior is still elusive. Researching the magneto-optical coupling would be helpful for understanding the axion electrodynamics and topological modulation of EuIn_2As_2 .

Here we use time-resolved magneto-optical Kerr effect (TR-MOKE) spectroscopy to study the spin wave excitation of EuIn_2As_2 . At low temperatures, as magnetic field increasing, spin dynamics begins to emerge after laser pulse pumping. A spin precession eigenmode at 18-GHz frequency is observed, which is different from the expected behavior in the presence of the easy plane, indicating the non-negligible contribution from high-order anisotropic energy. When the magnetization is saturated at the high field, the spin precession disappears whereas the coherent acoustic phonon mode (with a frequency of 35 GHz) emerges. In contrast with spin precession, the frequency of coherent acoustic phonon behaves independently on both temperature and field strength. The magnetic relaxation background shows a very long-lived process combing with a spike at time zero. By measuring the ultrafast dynamics of quasiparticles, we find no signature of coupling between magnetic order and the quasiparticle relaxation. We also ascertain that the coherent acoustic phonon is caused by the perturbation on magneto-optical coefficient, whereas the spike at time zero includes the additional contribution of demagnetization effect. Our findings provide the dynamical behavior of the spin and quasiparticle in EuIn_2As_2 after perturbation, which is helpful for the, subsequent, study on EuIn_2As_2 and related materials.

II. METHODS

Large single crystals of EuIn_2As_2 were grown by self-flux method, which is similar to that reported in early paper [6]. The magnetism of sample was characterized with a physical property measurement system. And the reflectivity spectroscopy was measured via a Fourier transform infrared spectrometer (Bruker IFS 80v). In the TR-MOKE measurement, the sample was mounted in an optical cryostat (SpectramagPT) with a base temperature of 1.6 K and a superconducting solenoid magnet up to 7 T. In all the measurements, the magnetic field was applied perpendicular to the ab plane of the sample. In time-resolved experiments, we used ultrafast laser with 800-nm wavelength, 1-kHz repetition rate, and 35-fs pulse duration. Pump beam wavelength was 400 nm (fluence was about $180 \mu\text{J}/\text{cm}^2$, generated by a

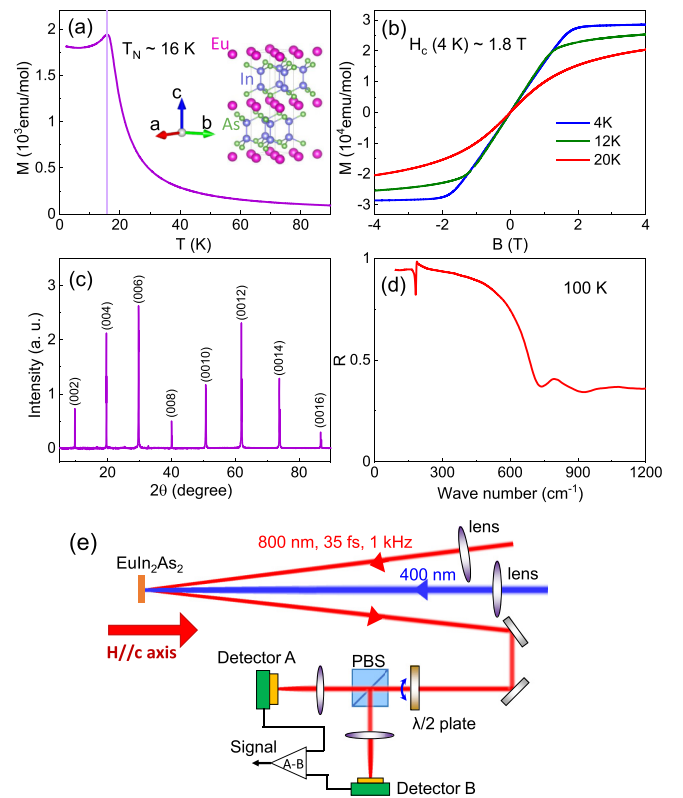


FIG. 1. The characterization of the EuIn_2As_2 sample and TR-MOKE experimental configuration. (a) Temperature-dependent magnetic susceptibility with an applied field of $H = 1000$ Oe along the c axis for the EuIn_2As_2 single crystal. The inset illustrates the crystal structure of EuIn_2As_2 . (b) Magnetic hysteresis (MH) loops with a field applied along the c axis at different temperatures where the saturation field can be identified to be 1.8 T at 3 K. (c) X-ray diffraction pattern of the EuIn_2As_2 single crystal. (d) In-plane reflectivity spectrum of EuIn_2As_2 below 1200 cm^{-1} . (e) Schematic of TR-MOKE measurement configurations.

barium metaborate crystal), and the probe beam wavelength was kept at 800 nm. Both the pump and the probe beams were linearly polarized and nearly normally illuminated on sample surface. The reflected probe beam passed through a half-wave plate and a beam-splitter cube, and finally detected by a pair of balanced photodiodes. The pump-induced change in Kerr rotation was determined as the value of the imbalance of these two photodiodes. At each field and temperatures, the full balancing between two photodiodes in the static state was executed. For the transient reflectivity measurement, only one photodiode was used at the 0-T field.

III. EXPERIMENTAL RESULTS

After synthesis, we first check the fundamental physical properties of the EuIn_2As_2 single crystal. As illustrated in Figs. 1(a) and 1(b), the magnetic susceptibility reveals the phase transition temperature $T_N = 16$ K and saturation field strength $H_s = 1.8$ T along the c axis, which is in agreement with early reports [6,12,14]. The x-ray-diffraction pattern represents sharp $(00L)$ peaks [Fig. 1(c)], which are well consistent with previous investigations [14], demonstrating the

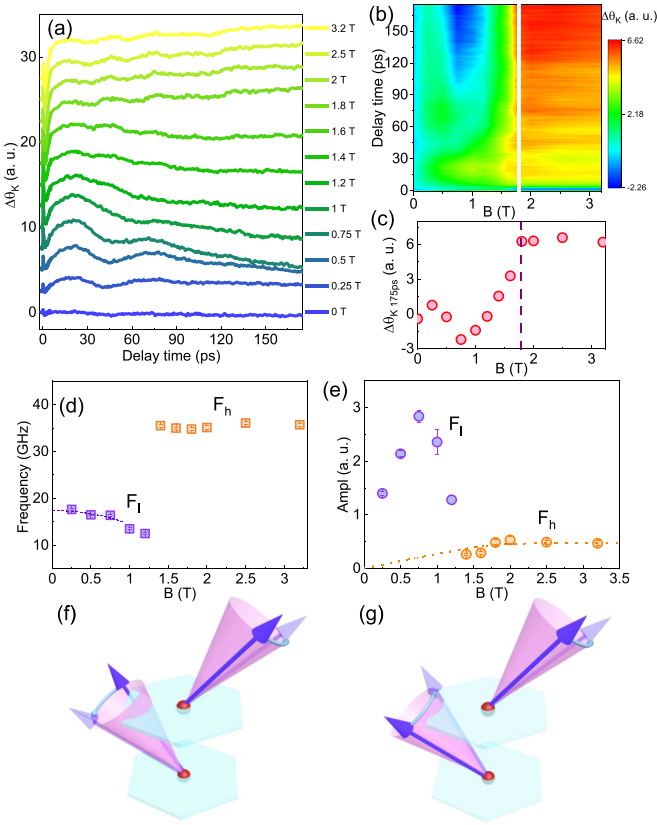


FIG. 2. Time dependence of spin dynamics under different applied magnetic fields at 3 K. (a) Time traces of $\Delta\theta_K$ with increasing magnetic field. (b) The two-dimensional color map of $\Delta\theta_K$ as a function of both magnetic field and delay time. The white solid line labels the saturation field strength. (c) The residual $\Delta\theta_K$ values at 175-ps delay time. The wine-red dashed line labels the transition. (d) Frequency of two modes at different magnetic fields. The dashed purple curve is the schematic of Eq. (1). (e) Magnetic-field evolution of amplitude of two oscillation modes. The orange dashed curve is rescaled MH relation at 4 K. (f) and (g) Schematic of two prospective spin precession eigenmodes in the AFM state.

pure phase of our sample. We also measured the reflectivity spectrum in range of 80–1200 cm^{-1} [shown in Fig. 1(d)]. The reported infrared-active phonon mode near 185 cm^{-1} and plasma edge near 700 cm^{-1} can be clearly seen [45], indicating a low carrier density metallic response. These characterizations all confirm the high quality of our EuIn_2As_2 sample.

After checking the sample, we performed the TR-MOKE measurements with applying different magnetic fields at 3 K where the experimental configuration is shown in Fig. 1(e). Figure 2(a) displays the time evolution of the pump-induced differential Kerr rotation ($\Delta\theta_K$) in the field range of 0–3.2 T. In the absence of an external magnetic field, there is almost no perturbation on Kerr rotation. When the magnetic field rises to 0.25 T, there is a sharp peak at time zero, then the Kerr rotation begins to increase and show a slow periodic modulation with a frequency of about 18 GHz (we call it F_l later). After 100 ps, the modulation becomes invisible, but $\Delta\theta_K$ still does not return to zero value. As the external field continues to increase, the amplitude of periodic modulation

slightly increases. Except for the oscillation component, the relaxation background exhibits a long-lived decay process with no signature of recovery at 175 ps. At 1.4 T, the second period of the oscillation cannot be resolved. When the magnetic field is further enhanced, the F_l mode completely vanishes, and another coherent oscillation mode occurs with a higher frequency of about 35 GHz (we call it F_h later). By applying the magnetic field up to 1.8 T, the F_h mode is strengthened. In the case of a stronger magnetic field, the temporal evolution of $\Delta\theta_K$ tends to stabilize.

We also plot the two-dimensional color map of a $\Delta\theta_K$ value as a function of both magnetic field and delay time in Fig. 2(b). From the color map, the magnetic evolution can be understood intuitively. In the range of 0–1.8 T, the intensity color is mostly green during the first 90 ps. With magnetic field increasing, it evolves from green to blue and back to green again in the 90–175-ps range and becomes red overall at 1.8 T. Above 1.8 T, the color alters independently on the magnetic field. Limited by the range of delay time, we roughly check the long-lived spin relaxation by extracting the $\Delta\theta_K$ value at 175-ps delay time as shown in Fig. 2(c). The $\Delta\theta_{K,175\text{ps}}$ value in Fig. 2(c) fluctuates slightly below 1 T, then rises rapidly and reaches a stable value above 1.8 T. This phenomenon corresponds to saturation of magnetization. And the critical magnetic field is consistent with that given by the susceptibility measurement.

We have extracted the frequency and amplitude of coherent oscillations in spin dynamics. As can be seen in Fig. 2(d), the frequency of F_l decreases continuously with the magnetic field. When the magnetic field is above 1.2 T, it is very difficult to obtain the frequency because only one period can be recognized. In magnetic materials, the spin dynamics behaviors are usually described by Landau-Lifshitz-Gilbert (LLG) equation [46]. If there are only two magnetic ions in a primitive magnetic cell (i.e., two-sublattice condition), the precession mode can be resolved in a succinct form. In general circumstances, the c axis is a hard axis, and the ab plane is an easy plane according to the lattice symmetry and in-plane AFM of EuIn_2As_2 . However, in this case the precession frequency is predicted harden with increasing field [46], which seems contradictory with our result. Interestingly, the precession eigenfrequency at a low field seems phenomenologically comparable with the relation in case of the field normal to the easy axis [the purple dashed curve in Fig. 2(d)],

$$\omega_{\text{low}} = \gamma \sqrt{H_A H_s - \frac{H_A}{H_s} H^2}, \quad (1)$$

where γ is the gyromagnetic ratio, H_A is the anisotropy field, H_s represents the assumed saturation field, and the subscript low means the one with lower frequency. The comparable result suggests easy directions (axes) on the ab plane. It is consistent with the observed spin flop with applying an in-plane field (implying a positive effective H_A) [12]. Considering the crystal symmetry, this in-plane anisotropy is most likely to originate from the higher-order free-energy term, $K_3 \sin^6(\theta) \cos(6\varphi)$ [46], where θ is the angle between c -axis and spin vector, and φ is the in-plane azimuthal angle. With negative K_3 , the zero-field equilibrium spin orientations are fixed to be ($\theta = \pi/2$, $\varphi = n\pi/3$) instead of an easy plane.

Therefore, at low field the spin precession behavior can be approximately described by Eq. (1). Where the strict solution of the precession frequency-field relation needs further investigation.

According to the LLG equation there should be the other spin precession mode [46]. However, it is invisible in our TR-MOKE measurement. This can be explained that the other frequency precession mode corresponds to antiphase couple between spins in adjacent layers and the projection of magnetization along the c axis is a nearly constant value [Fig. 2(g)]. For the F_h mode, it appears before the sample entering polarized paramagnetic (PP) state (i.e., below 1.8 T), and the frequency does not change with the magnetic field, thus, the spin precession origin [46] can be ruled out.

The field dependence of amplitude is also different in these two modes [Fig. 2(e)]. For low-energy mode F_l , the amplitude first increases and peaks in the vicinity of 0.75 T, then decreases with an increase of the magnetic field and soon becomes indistinguishable. For high-energy mode F_h , its amplitude first increases with the magnetic field and reaches saturation above 1.8 T, which is approximately proportional to magnetization [dashed curve in Fig. 2(e)], this phenomenon would be discussed later.

We also carried out the temperature-dependent TR-MOKE measurements both in AFM and in PP states. As illustrated in Fig. 3(a) when the magnetic field is 0.25 T, the precession period significantly gets longer with temperature increasing. Simultaneously, the amplitude of the oscillation decreases visually. The quantitative frequency-temperature relation is shown in Fig. 3(b). Figure 3(c) depicts the $\Delta\theta_K$ signal at 175-ps delay time.

In the PP state, the temperature evolution of spin dynamics manifests a distinct difference. Two negative relaxation components (one fast and one slow) can be seen in Fig. 3(d). When the sample temperature rises, the vertical offset of the slow component gradually decreases and finally disappears completely at 36 K. This can be roughly quantitatively reflected from the value of the $\Delta\theta_{K,175\text{ps}}$ signal [Fig. 3(f)]. The amplitude of the superimposed F_h mode also decreases with temperature increasing, but the frequency remains unchanged [Fig. 3(e)]. Note that both the oscillation mode and the offset of the $\Delta\theta_K$ signal survive above T_N , this may be caused by the surviving short-range magnetic order of Eu^{2+} ion above T_N , which will be discussed later.

To analyze the origin of this abnormal high-frequency mode F_h in the TR-MOKE measurement, we measure the transient reflectivity of EuIn_2As_2 below 40 K at 0 T where the result is shown in Fig. 4(a). The time traces of quasiparticle dynamics is totally different from spin dynamics. There are a negative fast decay component and a very slow positive component. These two processes have almost no change when the temperature rises across T_N . There is also a coherent oscillation superimposed on the relaxation process. The frequency of the oscillation does not change during the heating process, but the intensity decreases slightly [Fig. 4(b)], this is very typical of the acoustic phonon. Comparing with the F_h oscillation in the TR-MOKE measurement [Figs. 4(b) and 4(c)], they reach the extreme point of departure from equilibrium at same delay time. Thus, the oscillation mode with 35 GHz in $\Delta\theta_K(t)$ on the

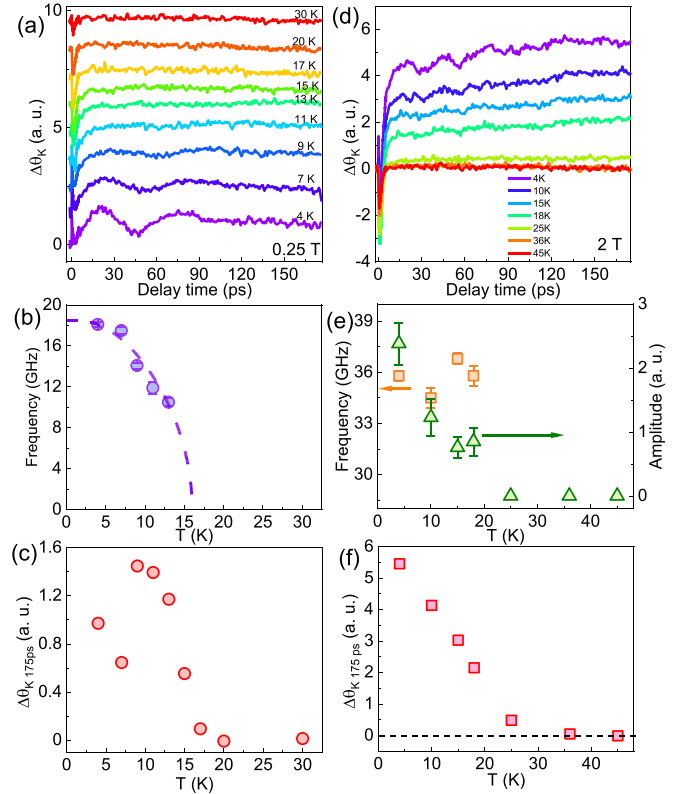


FIG. 3. Temperature-dependent TR-MOKE in AFM and PP states. (a) Temperature-dependent $\Delta\theta_K$ dynamics at $H = 0.25$ T. The data are offset for clarity. (b) The temperature evolution of precession frequency. The purple dashed curve is guide to the eyes. (c) The amplitudes of the $\Delta\theta_K$ signal at 175-ps delay time at different temperatures. (d) Temperature-dependent $\Delta\theta_K$ dynamics at $H = 2$ T. (e) The temperature evolution of high-energy oscillation frequency and amplitude. (f) The extracted amplitudes of the $\Delta\theta_K$ signal at 175-ps delay time at different temperatures from panel (d).

high magnetic field can be attributed to the coherent acoustic phonon.

IV. DISCUSSION

The observation of the acoustic phonon in the TR-MOKE measurement is relatively rare. And the spike-shaped signal at time zero is also discordant with following long-lived demagnetization process. The result is deserved to be discussed. In fact, the size of the Kerr rotation angle is determined by magnetization and magneto-optical coefficient [47]: $\theta_K = \alpha M$, where α is the (effective) magneto-optical coefficient. Hence, interpretation of the Kerr rotation should be as follows: $\Delta\theta_K = \Delta\alpha M + \alpha \Delta M$. Except for the real magnetic perturbation contribution ($\alpha \Delta M$), the optical contribution ($\Delta\alpha M$) is also included. A common causation of $\Delta\alpha$ is a photoinduced transient disturbance on state filling [34,47], which can be measured by pump-probe spectroscopy. Note that the $\Delta R/R$ and $\Delta\theta_K$ are comparable to a certain extent [the inset of Fig. 4(a)], both of them relax quickly on the picosecond scale, but there is still an obvious difference, thus, we attribute the fast decay component in the TR-MOKE to a combination of the

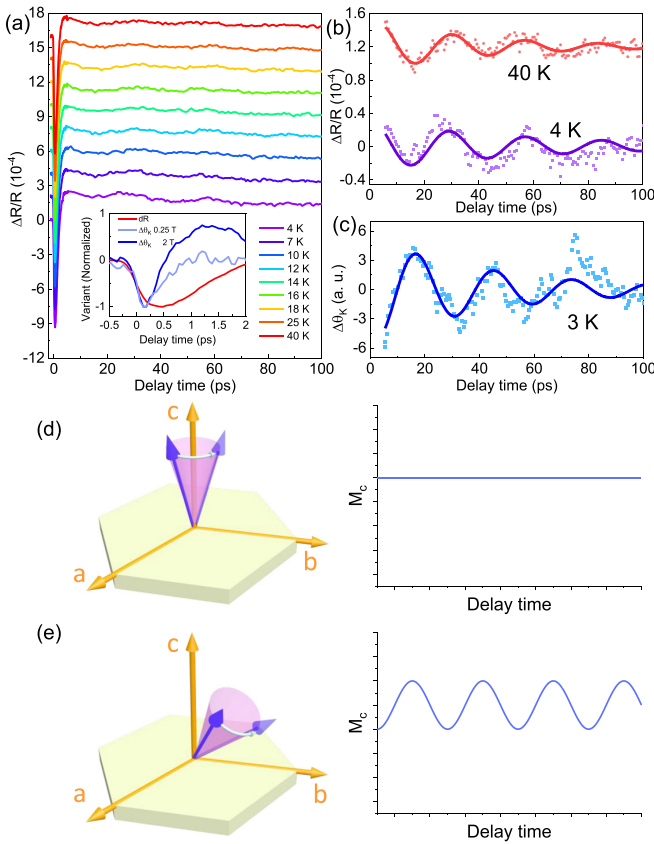


FIG. 4. Transient reflectivity and precession illustration in EuIn_2As_2 . (a) Transient reflectivity of EuIn_2As_2 below and above T_N where the coherent oscillations superimpose on relaxation background. The inset: comparison of normalized transient Kerr rotation (collected at 0.25 and 2 T) and reflectivity. (b) The extracted oscillations at 4 and 40 K from panel (a). (c) The corresponding coherent mode in the TR-MOKE measurements at 2 T. (d) The illustration of spin precession in the out-of-plane PP state. The spin vector rotates around the c axis and keeps the c -axis component invariant. (e) The illustration of spin precession in the transitional AFM-to-PP state. The spin vector rotates around a tilted equilibrium position and makes the c -axis component oscillate.

perturbation of magneto-optical coefficient and magnetic susceptibility instead of a single contribution. With the magnetic field increasing, the $\Delta\alpha M$ term is merely proportional to M and unchanged in time evolution. The $\alpha \Delta M$ term has a strong field dependence and evidently exhibits distinct behavior in AFM and PP states. The final magnetic-field dependence of the TR-MOKE signal is a cooperative result by these two terms.

Analogously, the acoustic phonon in the TR-MOKE measurement exhibit two characteristics: temperature- and field-independent frequency; and the similar field dependence of the amplitude to that of magnetization [Fig. 2(e)]. The

former feature excludes the possibility of coupling with magnetic order, and the latter confirms that the acoustic phonon signal comes from optical contribution $\Delta\alpha M$ (this term is proportional to magnetization M). From this point, the amplitude of the F_h mode can reflect the temperature evolution of field-induced magnetization M at 2 T. From Fig. 3(e), it can be seen that the amplitude of F_h vanishes above 25 K, implying the polarized paramagnetism is maintained below 25 K.

According to the LLG equation, in the PP state ($H > H_s$), the frequency of spin precession usually has an approximately linear relationship with the magnetic-field strength [46,48]. However, spin precession is not observed here above 1.8 T. In this case, the magnetic moments orient along the c axis. Therein, the spin precession eigenmode is assigned to rotating around the c axis [left panel of Fig. 4(d)]. With ignoring the decay of precession, the projection of magnetic moment on c axis (the dominant source of the MOKE signal [48]) is a constant [right panel of Fig. 4(d)], therefore, this precession pattern is unlikely to be detected in our experiments. Correspondingly, when the applied magnetic field is below H_s , the spin direction is tilted. After perturbation by laser pulse, the spin precesses around the new equilibrium position, and the intensity of the c -direction projection produces periodic changes [Fig. 4(e)], the oscillation on Kerr rotation is, therefore, detected.

V. CONCLUSION

To summarize, we investigate the spin dynamics in EuIn_2As_2 under different magnetic fields and temperatures. We observe a spin precession eigenmode in an unsaturated AFM state with a frequency of 18 GHz. Its abnormal magnetic dependence reveals the important contribution from high-order magnetic anisotropic energy. Such a low-frequency oscillation mode is difficult to be probed and investigated with other experimental methods. The transient demagnetization process with dramatic field dependence is also observed. Above 1.4 T, we find an acoustic phonon mode on the TR-MOKE measurement. After comparing with the quasiparticle dynamics, we confirm that the appearance of acoustic phonon mainly come from the perturbation on magneto-optical coefficient ($\Delta\alpha$). After saturation, the field-induced PP state is found to hold on up to 25 K. Our paper reveals the dynamical behavior of spin in EuIn_2As_2 and deepens the understanding of its magnetism, which is helpful for further investigation.

ACKNOWLEDGMENTS

We thank the helpful discussion with Prof. L. Yang and L. Liu. This work was supported by the National Natural Science Foundation of China (Grant No. 11888101), the National Key Research and Development Program of China (Grant No. 2022YFA1403901).

[1] H. Schäfer, B. Eisenmann and W. Müller, Zintl phases: transitions between metallic and ionic bonding, *Angew. Chem. Int. Ed. Engl.* **12**, 694 (1973).
 [2] S. M. Kauzlarich, *Special issue: Advances in zintl phases* **12**, 2554 (2019).

[3] D. M. Young and S. M. Kauzlarich, Preparation, structure, and electronic properties of $\text{Ca}_{11}\text{MSb}_9$ ($M = \text{Al, Ga, In}$), *Chem. Mater.* **7**, 206 (1995).
 [4] F. Gascoin, S. Ottensmahn, D. Stark, S. M. Haile, and G. J. Snyder, Zintl phases as thermoelectric materials: Tuned

- transport properties of the compounds $\text{Ca}_x\text{Yb}_{1-x}\text{Zn}_2\text{Sb}_2$, *Adv. Funct. Mater.* **15**, 1860 (2005).
- [5] D. Johrendt and R. Pöttgen, Superconductivity, magnetism and crystal chemistry of $\text{Ba}_{1-x}\text{K}_x\text{Fe}_2\text{As}_2$, *Physica C* **469**, 332 (2009).
- [6] A. M. Goforth, P. Klavins, J. C. Fettinger, and S. M. Kauzlarich, Magnetic properties and negative colossal magnetoresistance of the rare earth zintl phase EuIn_2As_2 , *Inorg. Chem.* **47**, 11048 (2008).
- [7] U. Subbarao and S. C. Peter, Crystal structure of YbCu_6In_6 and mixed valence behavior of Yb in $\text{YbCu}_{6-x}\text{In}_{6+x}$ ($x = 0, 1$, and 2) solid solution, *Inorg. Chem.* **51**, 6326 (2012).
- [8] S. R. Brown, S. M. Kauzlarich, F. Gascoin, and G. J. Snyder, $\text{Yb}_{14}\text{MnSb}_{11}$: New high efficiency thermoelectric material for power generation, *Chem. Mater.* **18**, 1873 (2006).
- [9] J. Yan, Z. Z. Jiang, R. C. Xiao, W. J. Lu, W. H. Song, X. B. Zhu, X. Luo, Y. P. Sun, and M. Yamashita, Field-induced topological hall effect in antiferromagnetic axion insulator candidate EuIn_2As_2 , *Phys. Rev. Res.* **4**, 013163 (2022).
- [10] T. Sato, Z. Wang, D. Takane, S. Souma, C. Cui, Y. Li, K. Nakayama, T. Kawakami, Y. Kubota, C. Cacho, T. K. Kim, A. Arab, V. N. Strocov, Y. Yao, and T. Takahashi, Signature of band inversion in the antiferromagnetic phase of axion insulator candidate EuIn_2As_2 , *Phys. Rev. Res.* **2**, 033342 (2020).
- [11] S. Regmi, M. M. Hosen, B. Ghosh, B. Singh, G. Dhakal, C. Sims, B. Wang, F. Kabir, K. Dimitri, Y. Liu, A. Agarwal, H. Lin, D. Kaczorowski, A. Bansil, and M. Neupane, Temperature-dependent electronic structure in a higher-order topological insulator candidate EuIn_2As_2 , *Phys. Rev. B* **102**, 165153 (2020).
- [12] Y. Zhang, K. Deng, X. Zhang, M. Wang, Y. Wang, C. Liu, J.-W. Mei, S. Kumar, E. F. Schwier, K. Shimada, C. Chen, and B. Shen, In-plane antiferromagnetic moments and magnetic polaron in the axion topological insulator candidate EuIn_2As_2 , *Phys. Rev. B* **101**, 205126 (2020).
- [13] S. X. M. Riberolles, T. V. Trevisan, B. Kuthanazhi, T. W. Heitmann, F. Ye, D. C. Johnston, S. L. Bud'ko, D. H. Ryan, P. C. Canfield, A. Kreyssig, A. Vishwanath, R. J. McQueeney, L. L. Wang, P. P. Orth, and B. G. Ueland, Magnetic crystalline-symmetry-protected axion electrodynamics and field-tunable unpinned Dirac cones in EuIn_2As_2 , *Nat. Commun.* **12**, 999 (2021).
- [14] F. H. Yu, H. M. Mu, W. Z. Zhuo, Z. Y. Wang, Z. F. Wang, J. J. Ying, and X. H. Chen, Elevating the magnetic exchange coupling in the compressed antiferromagnetic axion insulator candidate EuIn_2As_2 , *Phys. Rev. B* **102**, 180404 (2020).
- [15] Y. Xu, Z. Song, Z. Wang, H. Weng, and X. Dai, Higher-Order Topology of the Axion Insulator EuIn_2As_2 , *Phys. Rev. Lett.* **122**, 256402 (2019).
- [16] A. B. Sarkar, S. Mardanya, S.-M. Huang, B. Ghosh, C.-Y. Huang, H. Lin, A. Bansil, T.-R. Chang, A. Agarwal, and B. Singh, Magnetically tunable Dirac and Weyl fermions in the zintl materials family, *Phys. Rev. Mater.* **6**, 044204 (2022).
- [17] H. Zhang, C.-X. Liu, X.-L. Qi, X. Dai, Z. Fang, and S.-C. Zhang, Topological insulators in Bi_2Se_3 , Bi_2Te_3 and Sb_2Te_3 with a single Dirac cone on the surface, *Nat. Phys.* **5**, 438 (2009).
- [18] L. Fu, C. L. Kane, and E. J. Mele, Topological Insulators in Three Dimensions, *Phys. Rev. Lett.* **98**, 106803 (2007).
- [19] K. S. Novoselov, A. K. Geim, S. V. Morozov, D. Jiang, M. I. Katsnelson, I. V. Grigorieva, S. V. Dubonos, and A. A. Firsov, Two-dimensional gas of massless Dirac fermions in graphene, *Nature (London)* **438**, 197 (2005).
- [20] Y. L. Chen, J.-H. Chu, J. G. Analytis, Z. K. Liu, K. Igarashi, H.-H. Kuo, X. L. Qi, S. K. Mo, R. G. Moore, D. H. Lu, M. Hashimoto, T. Sasagawa, S. C. Zhang, I. R. Fisher, Z. Hussain, and Z. X. Shen, Massive Dirac fermion on the surface of a magnetically doped topological insulator, *Science* **329**, 659 (2010).
- [21] X. Wan, A. M. Turner, A. Vishwanath, and S. Y. Savrasov, Topological semimetal and Fermi-arc surface states in the electronic structure of pyrochlore iridates, *Phys. Rev. B* **83**, 205101 (2011).
- [22] S.-Y. Xu, I. Belopolski, N. Alidoust, M. Neupane, G. Bian, C. Zhang, R. Sankar, G. Chang, Z. Yuan, C.-C. Lee, S.-M. Huang, H. Zheng, J. Ma, D. S. Sanchez, B. Wang, A. Bansil, F. Chou, P. P. Shibayev, H. Lin, S. Jia *et al.*, Discovery of a Weyl fermion semimetal and topological Fermi arcs, *Science* **349**, 613 (2015).
- [23] B. Q. Lv, H. M. Weng, B. B. Fu, X. P. Wang, H. Miao, J. Ma, P. Richard, X. C. Huang, L. X. Zhao, G. F. Chen, Z. Fang, X. Dai, T. Qian, and H. Ding, Experimental Discovery of Weyl Semimetal TaAs, *Phys. Rev. X* **5**, 031013 (2015).
- [24] X.-L. Qi and S.-C. Zhang, Topological insulators and superconductors, *Rev. Mod. Phys.* **83**, 1057 (2011).
- [25] L. Fu and C. L. Kane, Superconducting Proximity Effect and Majorana Fermions at the Surface of a Topological Insulator, *Phys. Rev. Lett.* **100**, 096407 (2008).
- [26] E. Liu, Y. Sun, N. Kumar, L. Muechler, A. Sun, L. Jiao, S.-Y. Yang, D. Liu, A. Liang, Q. Xu, J. Kroder, V. Süß, H. Borrmann, C. Shekhar, Z. Wang, C. Xi, W. Wang, W. Schnelle, S. Wirth, Y. Chen *et al.*, Giant anomalous hall effect in a ferromagnetic kagome-lattice semimetal, *Nat. Phys.* **14**, 1125 (2018).
- [27] P. Li, J. Koo, W. Ning, J. Li, L. Miao, L. Min, Y. Zhu, Y. Wang, N. Alem, C.-X. Liu, Z. Mao, and B. Yan, Giant room temperature anomalous hall effect and tunable topology in a ferromagnetic topological semimetal Co_2MnAl_3 , *Nat. Commun.* **11**, 3476 (2020).
- [28] D. F. Liu, A. J. Liang, E. K. Liu, Q. N. Xu, Y. W. Li, C. Chen, D. Pei, W. J. Shi, S. K. Mo, P. Dudin, T. Kim, C. Cacho, G. Li, Y. Sun, L. X. Yang, Z. K. Liu, S. S. P. Parkin, C. Felser, and Y. L. Chen, Magnetic Weyl semimetal phase in a kagomé crystal, *Science* **365**, 1282 (2019).
- [29] I. Belopolski, K. Manna, D. S. Sanchez, G. Chang, B. Ernst, J. Yin, S. S. Zhang, T. Cochran, N. Shumiya, H. Zheng, B. Singh, G. Bian, D. Multer, M. Litskevich, X. Zhou, S.-M. Huang, B. Wang, T.-R. Chang, S.-Y. Xu, A. Bansil *et al.*, Discovery of topological Weyl fermion lines and drumhead surface states in a room temperature magnet, *Science* **365**, 1278 (2019).
- [30] Z. K. Liu, L. X. Yang, S.-C. Wu, C. Shekhar, J. Jiang, H. F. Yang, Y. Zhang, S.-K. Mo, Z. Hussain, B. Yan, C. Felser, and Y. L. Chen, Observation of unusual topological surface states in half-Heusler compounds LnPtBi ($\text{Ln}=\text{Lu}, \text{Y}$), *Nat. Commun.* **7**, 12924 (2016).
- [31] A. M. Essin, J. E. Moore, and D. Vanderbilt, Magnetolectric Polarizability and Axion Electrodynamics in Crystalline Insulators, *Phys. Rev. Lett.* **102**, 146805 (2009).
- [32] D. Zhang, M. Shi, T. Zhu, D. Xing, H. Zhang, and J. Wang, Topological Axion States in the Magnetic Insulator MnBi_2Te_4 with the Quantized Magnetolectric Effect, *Phys. Rev. Lett.* **122**, 206401 (2019).
- [33] C. Liu, Y. Wang, H. Li, Y. Wu, Y. Li, J. Li, K. He, Y. Xu, J. Zhang, and Y. Wang, Robust axion insulator and Chern

- insulator phases in a two-dimensional antiferromagnetic topological insulator, *Nature Mater.* **19**, 522 (2020).
- [34] A. Barman and J. Sinha, *Spin Dynamics and Damping in Ferromagnetic Thin Films and Nanostructures* (Springer, Berlin, 2018).
- [35] L. Yang, N. A. Sinitsyn, W. Chen, J. Yuan, J. Zhang, J. Lou, and S. Crooker, Long-lived nanosecond spin relaxation and spin coherence of electrons in monolayer MoS₂ and WS₂, *Nat. Phys.* **11**, 830 (2015).
- [36] B. Huang, G. Clark, E. Navarro-Moratalla, D. R. Klein, R. Cheng, K. L. Seyler, D. Zhong, E. Schmidgall, M. A. McGuire, D. H. Cobden, W. Yao, D. Xiao, P. Jarillo-Herrero, and X. Xu, Layer-dependent ferromagnetism in a van der waals crystal down to the monolayer limit, *Nature (London)* **546**, 270 (2017).
- [37] C. Gong, L. Li, Z. Li, H. Ji, A. Stern, Y. Xia, T. Cao, W. Bao, C. Wang, Y. Wang, Z. Q. Qiu, R. J. Cava, S. G. Louie, J. Xia, and X. Zhang, Discovery of intrinsic ferromagnetism in two-dimensional van der waals crystals, *Nature (London)* **546**, 265 (2017).
- [38] J. Xia, Y. Maeno, P. T. Beyersdorf, M. M. Fejer, and A. Kapitulnik, High Resolution Polar Kerr Effect Measurements of Sr₂RuO₄: Evidence for Broken Time-Reversal Symmetry in the Superconducting State, *Phys. Rev. Lett.* **97**, 167002 (2006).
- [39] Y. Okamura, S. Minami, Y. Kato, Y. Fujishiro, Y. Kaneko, J. Ikeda, J. Muramoto, R. Kaneko, K. Ueda, V. Kocsis, N. Kanazawa, Y. Taguchi, T. Koretsune, K. Fujiwara, A. Tsukazaki, R. Arita, Y. Tokura, and Y. Takahashi, Giant magneto-optical responses in magnetic Weyl semimetal Co₃Sn₂S₂, *Nat. Commun.* **11**, 4619 (2020).
- [40] A. Kirilyuk, A. V. Kimel, and T. Rasing, Ultrafast optical manipulation of magnetic order, *Rev. Mod. Phys.* **82**, 2731 (2010).
- [41] E. Beaurepaire, J.-C. Merle, A. Daunois, and J.-Y. Bigot, Ultrafast Spin Dynamics in Ferromagnetic Nickel, *Phys. Rev. Lett.* **76**, 4250 (1996).
- [42] G. P. Zhang and W. Hübner, Laser-Induced Ultrafast Demagnetization in Ferromagnetic Metals, *Phys. Rev. Lett.* **85**, 3025 (2000).
- [43] M. van Kampen, C. Jozsa, J. T. Kohlhepp, P. LeClair, L. Lagae, W. J. M. de Jonge, and B. Koopmans, All-Optical Probe of Coherent Spin Waves, *Phys. Rev. Lett.* **88**, 227201 (2002).
- [44] G. V. Astakhov, A. V. Kimel, G. M. Schott, A. A. Tsvetkov, A. Kirilyuk, D. R. Yakovlev, G. Karczewski, W. Ossau, G. Schmidt, L. W. Molenkamp, and T. Rasing, Magnetization manipulation in (Ga,Mn)As by subpicosecond optical excitation, *Appl. Phys. Lett.* **86**, 152506 (2005).
- [45] B. Xu, P. Marsik, S. Sarkar, F. Lyzwa, Y. Zhang, B. Shen, and C. Bernhard, Infrared study of the interplay of charge, spin, and lattice excitations in the magnetic topological insulator EuIn₂As₂, *Phys. Rev. B* **103**, 245101 (2021).
- [46] A. G. Gurevich and G. A. Melkov, *Magnetization Oscillations and Waves* (CRC, Boca Raton, FL, 1996).
- [47] I. Razdolski, A. Alekhin, U. Martens, D. Bürstel, D. Diesing, M. Münzenberg, U. Bovensiepen, and A. Melnikov, Analysis of the time-resolved magneto-optical kerr effect for ultrafast magnetization dynamics in ferromagnetic thin films, *J. Phys.: Condens. Matter* **29**, 174002 (2017).
- [48] X.-X. Zhang, L. Li, D. Weber, J. Goldberger, K. F. Mak, and J. Shan, Gate-tunable spin waves in antiferromagnetic atomic bilayers, *Nature Mater.* **19**, 838 (2020).